Reversals and collisions optimize protein exchange in bacterial swarms

Aboutaleb Amiri
Department of Physics, University of Notre Dame, Notre Dame, Indiana 46556, USA

Cameron Harvey
Department of Applied and Computational Mathematics and Statistics, University of Notre Dame, Notre Dame, Indiana 46556, USA

Amy Buchmann
Department of Mathematics, Tulane University, New Orleans, Louisiana 70118, USA

Scott Christley
UT Southwestern Medical Center, Dallas, Texas 75390, USA

Joshua D. Shrout
Department of Civil and Environmental Engineering, University of Notre Dame, Notre Dame, Indiana 46556, USA

Igor S. Aranson
Department of Biomedical Engineering, Pennsylvania State University, University Park, Pennsylvania 16802, USA and Materials Science Division, Argonne National Laboratory, Argonne, Illinois 60439, USA

Mark Alber*
Department of Applied and Computational Mathematics and Statistics, University of Notre Dame, Notre Dame, Indiana 46556, USA and Department of Mathematics, University of California, Riverside, California 92521, USA

(Received 25 April 2016; revised manuscript received 18 February 2017; published 13 March 2017)

Swarming groups of bacteria coordinate their behavior by self-organizing as a population to move over surfaces in search of nutrients and optimal niches for colonization. Many open questions remain about the cues used by swarming bacteria to achieve this self-organization. While chemical cue signaling known as quorum sensing is well-described, swarming bacteria often act and coordinate on time scales that could not be achieved via these extracellular quorum sensing cues. Here, cell-cell contact-dependent protein exchange is explored as a mechanism of intercellular signaling for the bacterium *Myxococcus xanthus*. A detailed biologically calibrated computational model is used to study how *M. xanthus* optimizes the connection rate between cells and maximizes the spread of an extracellular protein within the population. The maximum rate of protein spreading is observed for cells that reverse direction optimally for swarming. Cells that reverse too slowly or too fast fail to spread extracellular protein efficiently. In particular, a specific range of cell reversal frequencies was observed to maximize the cell-cell connection rate and minimize the time of protein spreading. Furthermore, our findings suggest that predesigned motion reversal can be employed to enhance the collective behavior of biological synthetic active systems.

DOI: 10.1103/PhysRevE.95.032408

I. INTRODUCTION

The ability of living organisms to self-organize their movement is seen throughout nature, from herds of large mammals to flocks of birds, schools of fish, and swarms of insects. This organization emerges from local interactions between individuals within the population. Leaderless, self-organized movement, commonly referred to as collective motion, is an active area of research that bridges biology, physics, mathematics, and computer science (see, among others, Ref. [1]). Remarkably, patterns of collective locomotion can be seen even in the simplest forms of life, such as bacteria. While bacteria are essentially single-cell containers of DNA that are "wired" to eat, grow, and reproduce, their genetic programming allows them to interact with each other by exchanging chemical signals and proteins and to respond to their environmental changes, resulting in the emergence of complicated multicellular behavior that is crucial to their survival.

While chemical cue signaling known as quorum sensing is well described, swarming bacteria often act and coordinate on time scales that could not be achieved via these extracellular quorum sensing cues [2]. Cell-cell contact-dependent protein exchange is explored in this paper as a possible mechanism of bacterial self-organization using well-known social bacterium *Myxococcus xanthus* as an example. Spreading of protein by swarming bacteria can be compared to people at a party randomly exchanging information with one another in a small group, then moving on to another small group. How long it will take to inform everyone depends on the population structure, its density, and the specific strategy of the information exchange. We used Shannon entropy [3] to measure the level of protein spreading in the population of bacteria. This approach can be applied to investigate any molecular exchange between cells that make transient contact with each other. For

*malber@ucr.edu

example, Shannon entropy has been used to study biochemical signaling between rod-shaped self-propelled bacteria as an information transmission problem [4]. It was also used to characterize the collective motion of animal groups [5,6], diversity of species [7], and diversity in bacterial and archaeal DNA [8], and, in a more physical context, to study interacting nonconservative units such as bubbles in foam [9].

Myxobacteria are common soil bacteria that are among the most "social" bacteria in nature [10,11]. *M. xanthus* is the most studied of the myxobacteria, which were used extensively to explore collective behavior. It is known that individual *M. xanthus* cells regularly reverse their direction of motion [12], which has an important impact on the swarming expansion rate of the colony [13]. It has been observed that certain outer membrane lipoproteins can be transferred from one cell to another by direct contact between cells. This contact-mediated transfer is sufficient to restore function in mutants that are deficient for these specific proteins [14–18]. Yet a role for protein exchange as a mechanism to stimulate social behavior and collective motion has not been determined.

Experimental results on *M. xanthus* protein exchange can be summarized as follows. It is known that cells exchange proteins related to signaling during the development of *M. xanthus* fruiting bodies under starvation, resulting in some cells differentiating into spores [19–23]. Also, lipoproteins related to the motility of cells, such as Tgl, CglB, and CglC, can be exchanged to restore gliding motility under nutrient-rich conditions [17,18,24]. *M. xanthus* cells lacking motility genes are able to acquire these proteins when in contact with cells expressing them, and they become motile through a process known as stimulation. At least one of the cells (donor, recipient, or even another cell that is not directly involved in the outer membrane protein exchange) must be motile to facilitate the transfer [2,25]. Outer membrane exchange can also enable predation [26–28] and the repair of damaged or deficient outer membranes of cells [29]. It has been shown that *M. xanthus* cells with different levels of outer membrane material that come into direct contact share efficiently an equal amount of outer membrane material within a relatively short period of time [17,24,30–32].

While the physical properties of *M. xanthus* have been partially characterized in experiments [33,34], *in vivo* modification of flexibility or adhesion strength in a deliberate and controlled way in mutants cannot be easily done at this time. Changing parameters in computer simulations provides one with a fast and efficient way of producing and testing different hypotheses. Computational modeling of *M. xanthus* swarming and collective behavior has previously focused on the emergence of cell clusters and patterns within a bacterial population [35–38].

This paper demonstrates that the newly proposed bacterial mechanism that maintains and combines experimentally observed ranges of reversal periods, the flexibility of bacteria, and slime capsule adhesivity optimizes protein spreading in the myxobacterial population. This mechanism, which evolved as a result of evolution, determines the number and duration of cell-cell connections between swarming rod-shaped self-propelled bacteria resulting in the ability of a colony of swarming bacteria to efficiently spread protein. This benefits the whole population through an increase in rescuing nonmotile bacteria and coordinating the self-organized motion of bacteria during predation and fruiting body formation. To test the mechanism, the subcellular element (SCE) model of bacterial swarming [39] was extended by incorporating novel submodel simulating cell-cell protein transfer, and extensive model simulations were conducted. The model was first calibrated using experimental data. To perform simulations involving a large number of cells, computational implementation of the extended SCE model has been parallelized on the cluster of graphical processing units (GPUs).

II. BIOLOGICALLY CALIBRATED COMPUTATIONAL MODEL

The SCE method has been introduced to study multicellular systems [40], and it was used to model epithelial cell growth [41], platelets in blood flow [42,43], and gliding bacteria [39]. In this approach, cells are represented as a collection of interconnected subcellular elements. The dynamics of each SCE results from the elastic forces in response to changes in cell shape or cell-cell and cell-environment interactions. The SCE model of bacterial swarming developed in [39] takes into account adhesive forces between cells and the substrate they move on as well as the flexibility of individual cells and the frequency of reversals. The inclusion of adhesion and reversal periods in this computational model sets this approach apart from [35–37,44].

In this paper, an extended version of our previous model introduced in [39] is used. The model is designed to study A+S- *M. xanthus* mutants, which use only an A- (adventurous) motility engine that enables them to move on their own on the surface, but lack an S- (social) motility engine, which utilizes type IV pili to attach bacteria to neighboring cells and move together with them. We model these mutants because it enables us to focus on protein exchange between self-propelled bacteria without interference from the S-motility engine.

In the model, cells are represented by 16 interconnected SCEs, and to model the cell motion due to slime A-motility on individual SCEs, a distributed force engine is used. The distributed force engine is implemented by applying force to every fourth element of the cells. We assume that each cell interacts with the substrate through an adhesive force representing a slime capsule interaction with the substrate. Cells reverse their motion direction by switching which cell pole is identified as the head and tail, thus switching the direction of the forces (F_s) applies on the elements. The directional change is controlled by an internal reversal clock assigned to every cell with the fixed reversal period (t_r). The reversal clock time increases at every simulation step until it reaches t_r. Reflecting boundary conditions are implemented in the simulations. Cells in our computational model are assumed, based on experimental observations, to be 5 μm in length with an aspect ratio of 10:1. A random noise in the direction of cell movement, $\mathbf{R}(t) = k_{\text{rand}}\ \zeta$, is used to model the intrinsic motility fluctuation of bacteria gliding on agar. ζ is a normally distributed random vector. Because these bacteria glide in a highly viscous slime, we can make the simplifying assumption that inertial effects can be neglected, resulting in the following

TABLE I. Default values of the parameters used in simulations.

Parameter	Value
Cell width	0.5 μm
Cell length	5 μm
Compressibility k_b	148.0 fJ μm^{-2}
Flexibility k_θ	0.01 fJ
Friction coefficient γ	1.0×10^{-5} nN μs μm^{-1}
Cell-cell adhesion ϵ	0.01 fJ
Repulsion distance λ_{ij}	0.5 μm
Adhesion distance $\mathrm{LJ}_{\mathrm{cutoff}}$	0.6 μm
Reversal period t_r	480 s
Slime force F_s	120 pN
Head noise k_{rand}	0.1
Protein exchange rate R_p	0.003 s^{-1}
Number of cells N	512
Size of domain $L_x \times L_y$	100×100 μm^2

form of the equation of motion:

$$\frac{d}{dt}\mathbf{x}(t) = \frac{1}{\gamma}[\mathbf{R}(t) - \nabla U(\mathbf{x}(t))]. \quad (1)$$

Biologically calibrated model parameters are provided in Table I.

Reversal periods and the length and width of bacteria were measured by tracking *M. xanthus* cells in *in vivo* experiments. The dynamic curvature analysis algorithm was used to measure changes in the shapes of cells when they collided with each other. A comparison between these measurements for *in vivo* and *in silico* experiments was used in [39] to calibrate the values of different model parameters determining the level of flexibility, compressibility, cell-cell, and cell-substrate adhesion as well as the magnitude of the force produced by the A-motility engine. The rate of protein exchange is set specifically for motility proteins such as Tgl, CglB, and CglC based on reported experimental observations [17,24,31,32].

III. EVALUATION OF PROTEIN SPREADING USING SHANNON ENTROPY

To test how different physical and behavioral properties could affect protein spreading within a population of bacteria, in each simulation the level of protein on cells is initialized from a uniformly random distribution on the interval [0, 1]. This is done to mimic experiments in which cells are tagged with a fluorescent protein, and the transfer of this protein is visualized [17,24,31,32]. Experimental observations show that contacting cells share their protein efficiently within a few minutes, and the rate of protein exchange R_p is set accordingly in our simulations. Two cells are characterized as being connected in our simulations if the smallest distance between their SCEs is less than 0.6 μm. This accounts for the width of a cell (0.5 μm) and the slime capsule surrounding the cell (0.1 μm). An exchange of protein is carried out when two cells are in contact, with the constant rate from the cell with the higher value to the cell with the lower value. Thus, the average value of protein is assumed to remain constant throughout the simulation, and the distribution of protein converges to the average protein level of the population.

We use in this paper the concept of Shannon entropy from information theory [3] to determine the efficiency of the protein exchange in populations of cells with different physical properties. Simply put, the closer a population gets to the state with each cell having the same amount of protein, the larger the entropy of the system becomes. The entropy of the population of cells calculated at time t is $I(t) = -\sum_k \tilde{n}(k)\log(\tilde{n}(k))$, where $\tilde{n}(k) = n_k/n_{\mathrm{tot}}$ is the distribution of the protein level (n_k) normalized by the total amount of protein in the population (n_{tot}). $I(t)$ is always non-negative. To see how evenly protein is distributed in the population, we calculate the normalized value of the change of the entropy $\widetilde{\Delta I}(t) = [I(t) - I(0)]/E$. The normalization factor $E = I(\infty) - I(0)$ is the change in the entropy of the system if it starts with a uniformly random distribution $n_k \in [0,1]$ and eventually reaches the state where the level of protein in every cell is equal to the average value $n_k = 0.5$. (See the Appendixes for more details on entropy calculations.)

IV. RESULTS

In what follows, we identify a range of reversal frequencies and physical properties of *M. xanthus*, optimizing the ability of the population to make cell-cell connections and spread proteins. We perform simulations to test the effect of varying one parameter while keeping the others constant to their biologically calibrated values (see Table I).

A. Cell-cell connection rate and duration

Distribution of reversal periods observed in experiments was presented in [13] (see Fig. 1). Most of the experimentally observed reversal periods were between 4 and 12 min (~77%) with a skew toward shorter reversal periods in that range even though the average reversal period was between 8 and 9 min.

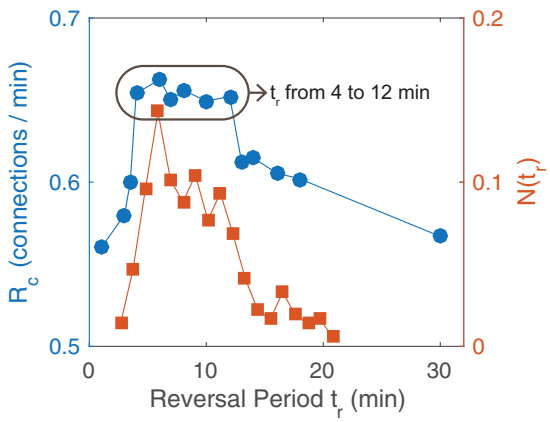

FIG. 1. Dependence of the R_c on reversal periods. Solid circles represent R_c for populations in simulations with different reversal periods. R_c for the population of nonreversing cells was measured to be of the order of 0.46 connections/min. The filling fraction in the simulations was set at 12.8% close to the average fraction observed in experiments at the swarm edge. Solid squares display the distribution of reversal periods within a population of bacteria in an experiment obtained by calculating the fraction of observed bacteria $N(t_r)$ that reverse with period t_r (adopted from [13]).

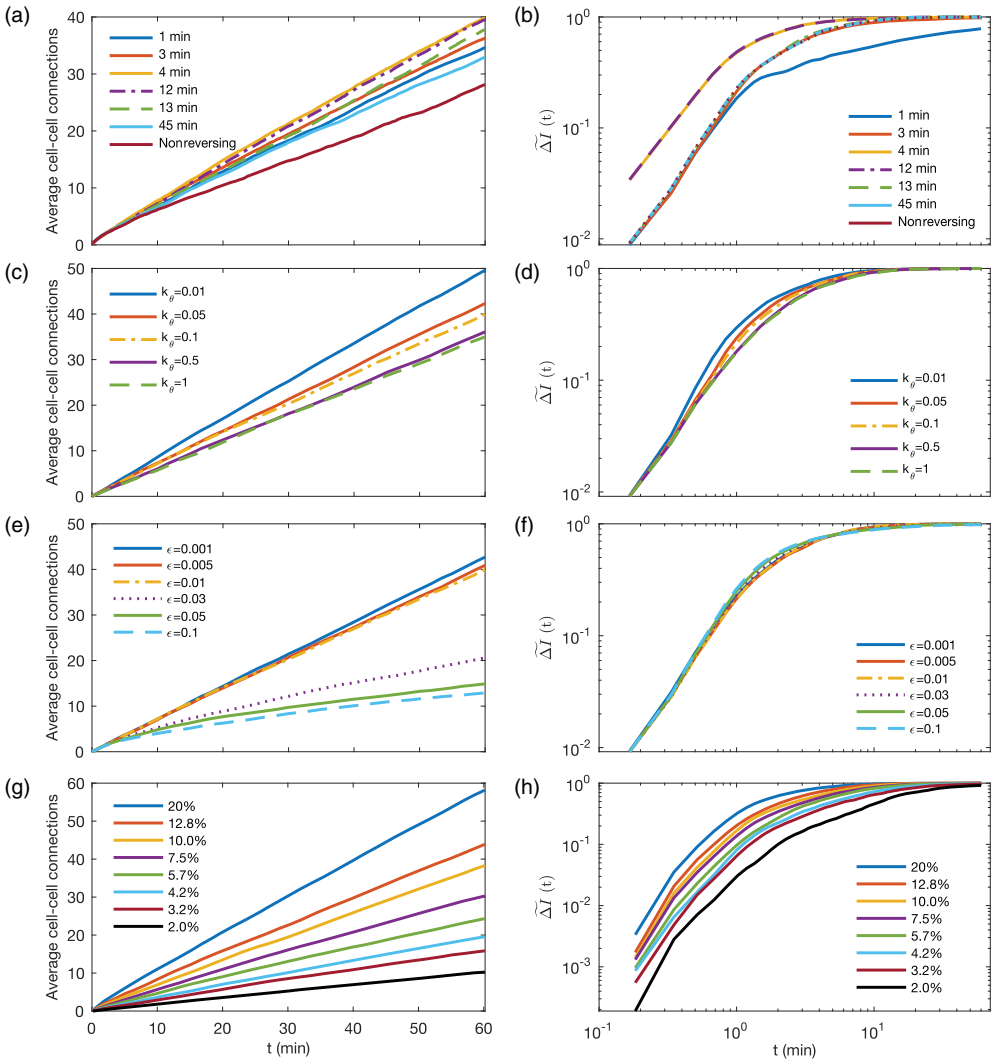

FIG. 2. (a), (c), (e), and (g) Dependence of the average number of cell-cell connections on reversal frequency, flexibility, adhesion, and filling fraction, respectively. (b), (d), (f), and (h) Change of the normalized Shannon entropy $\widetilde{\Delta I}(t)$ characterizing the distribution of protein over time in bacterial populations with different reversal frequencies, cell flexibilities, cell-cell adhesions, and filling fraction, respectively. (See the Appendixes for details about measurement and normalization of entropy.)

Very few cells (∼6%) reversed in less than 4 min, while some (∼17%) reversals took more than 12 min.

Reversal period t_r is varied in our simulations from 1 to 30 min. The cumulative number of cell-cell connections (without repeated connections) is calculated for each cell and is averaged over all cells in the population at time t, resulting in the average number of cell-cell connections. The rate of cell-cell connections R_c is calculated using a linear fit to the average number of cell-cell connections as a function of time. The average connection duration $\tau = \sum_{ev=1}^{N_{\rm tot}} w(ev)D(ev)$ is calculated for $N_{\rm tot} = 10^4$ collision events, where $w(ev)$ is the weight for each event (the number of occurrences divided by $N_{\rm tot}$). $D(ev)$ is the duration of each event. Simulations showed that populations with reversal frequencies in the experimental range had a maximal rate of cell-cell connections (Fig. 1). For example, the population of cells that reversed with a period from the experimentally observed range of 4–12 min made connections with the rate $R_c = 0.65 \pm 0.01$ min^{-1}, which was 14% more than R_c of the population of cells reversing every minute and 41% more than R_c for the population of cells that did not reverse at all. Figure 2(a) shows the average number of cell-cell connections over t min for different reversal periods. The results showed very similar behavior for all the reversal periods within the range from 4 to 12 min. Therefore, we only show the results for the end points of this range in Figs. 2(a) and 2(b).

Our simulations also predict (see Fig. 2) that, as the reversal period t_r increases, two important transitions occur between the following three different phases: (i) nonmotile state, (ii) effective swarming state, and (iii) jammed state. Namely, increasing the reversal period from a very low value ($t_r = 1$ min) to the values in the experimentally observed range (t_r from 4 to 12 min) results in the increased ability of bacteria to effectively move in one direction, which results in an increased rate of cell-cell connections R_c. A further increase of t_r above the experimental range causes the formation of traffic jams and reduces R_c since the bacteria that are stuck in traffic jams cannot explore the domain efficiently and make new cell-cell

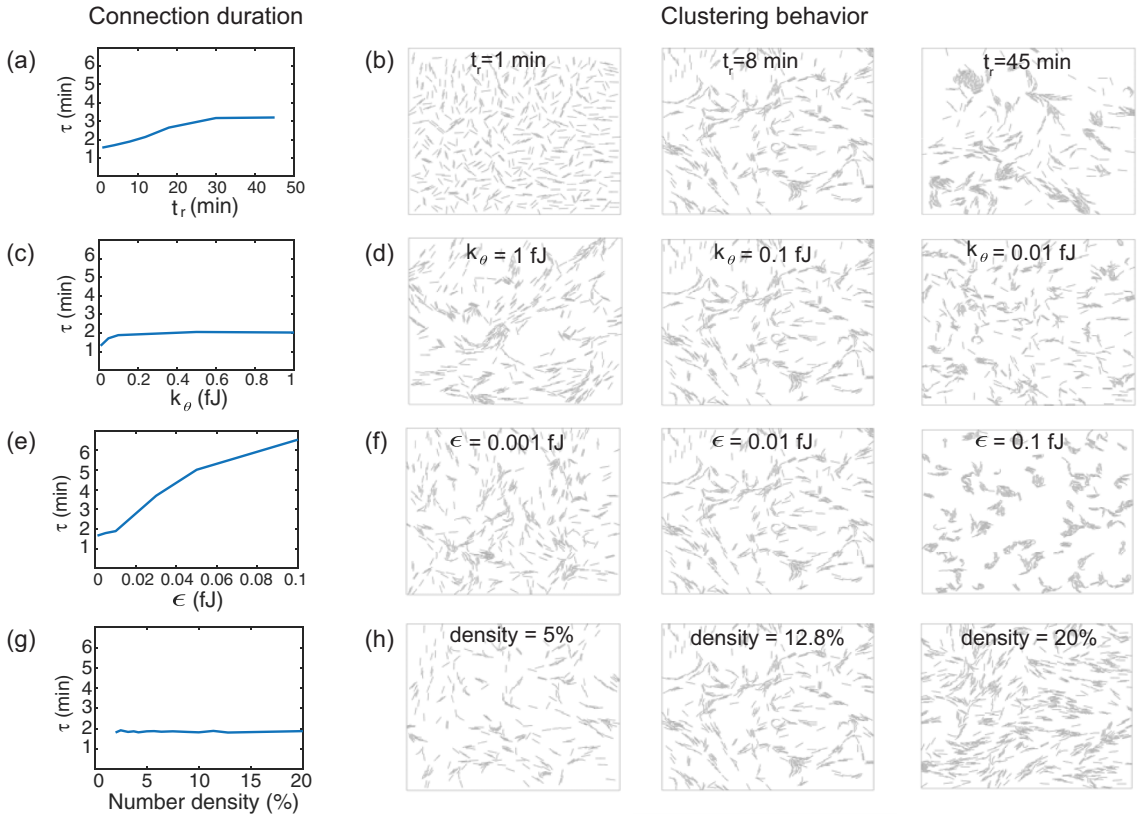

FIG. 3. (a), (c), (e), and (g) Dependence of the average connection duration on the reversal period, bending rigidity, adhesion strength, and number density, respectively. (b), (d), (f), and (h) Clustering behavior for different (low, calibrated with experiments, and high) values of reversal period, bending rigidity, adhesion strength, and number density, respectively.

connections. Qualitative evidence to support this hypothesis is given in the snapshot of the simulations in Fig. 3(b). The phase transition as a result of varying filling fraction has been previously studied for a population of self-propelled rod-shaped bacteria with directional reversals [45].

Model simulations also showed that experimentally observed levels of cell flexibility maximized the rate of cell-cell connections and the spread of protein in the population. Cell rigidity was varied from the high level (corresponding to the bending stiffness constant $k_\theta = 1$ fJ [one femtojoule (fJ), a unit of bending or adhesion energy, is equal to 10^{-15} J]) to the very low level (with $k_\theta = 0.01$ fJ). The values of the bending stiffness less than this range ($k_\theta < 0.01$ fJ) caused cells in the simulations to bend to the extent that they started forming loops and knots [39]. We consider this to be nonbiological behavior since cells have not been observed to form loops and knots in the experiments. Using values higher than this range would not change the rigidity of cells any further (see [39] for details on model calibration). Figure 2(c) demonstrates that cells with the experimentally calibrated value of the flexibility parameter ($k_\theta = 0.01$ fJ) have a connection rate that is 42% bigger than that for rigid cells ($k_\theta = 1$ fJ). This occurs because more flexible cells have a slightly higher collision cross section due to bending, and they explore space more efficiently than rigid cells, resulting in the increased rate of cell-cell connections. Furthermore, the direction of motion of more flexible cells can be perturbed (as a result of interaction with the environment) more easily due to a lower cost of energy. Once a cell that is adhered to a cluster of cells experiences this change in the direction of motion, it can split from the cluster and travel until it reaches another cluster and starts making new connections. Variation of the bending rigidity parameter k_θ was shown to have a negligible impact on the average connection duration [Fig. 3(c)] and clustering behavior [Fig. 3(d)].

Next, the impact of cell-cell adhesion on the connection rate was investigated. Adhesion force between two contacting cells comes from the interaction between capsular polysaccharide that covers bacterial bodies. Figure 2(e) shows that weaker adhesive interaction between cells (lower ϵ) results in a considerably higher connection rate. Cells with the experimentally calibrated value of the cell-cell adhesion parameter ($\epsilon = 0.01$ fJ) make connections at a rate that is 15% less than the rate of less adhesive cells (with $\epsilon = 0.001$ fJ) and 2.29 times the connection rate of more adhesive cells (with $\epsilon = 0.1$ fJ). This occurs because strong cell-cell adhesion results in cells holding onto each other more effectively, sequestering them from the rest of the population. We found that with the increase in the value of the parameter that controls the strength of cell-cell adhesion from $\epsilon = 0.01$ to 0.03 fJ, the rate of cell-cell connections decreased sharply as a result of a significant increase in connection duration [Fig. 3(e)]. Namely, the duration of a cell-cell connection exceeded the time it took for them to exchange protein efficiently, resulting in a reduction in the number of new cell-cell connections.

The average rate of cell-cell connections R_c was also shown to increase as a result of increasing the population

number density defined as the two-dimensional filling fraction [Fig. 2(g)]. This happens because bacteria in populations with a higher number density (20%) spend considerably less time (approximately 4.4 times less) moving freely before making contact with another cell compared to the cells in a population with number density 2%. Figure 3(g) demonstrates that varying the filling fraction does not have a significant impact on the duration of connections, and that improved efficiency of protein spreading is mainly due to the increased rate of cell-cell connections.

B. Evaluation of protein spreading efficiency

To quantify the efficiency of protein transfer, we used the Shannon entropy as a metric indicating the amount of uncertainty in the level of protein in each cell in the population. The simulation results are represented for different reversal periods [Fig. 2(b)], levels of flexibility [Fig. 2(d)], and adhesion [Fig. 2(f)], while all other parameter values were fixed to their experimentally calibrated values listed in Table I. The entropy of the population eventually approached the same maximum value in all simulations, but over different time intervals. Therefore, the time required for a system to reach half the maximum entropy was used as a measure of the efficiency of protein spreading.

The optimal efficiency of protein transfer was obtained for reversal periods in the range observed in experiments from 4 to 12 min. In extreme cases of nonreversing cells or cells reversing very frequently, protein spreading efficiency drops dramatically [see Fig. 2(b)]. This happens because cells that reverse with periods less than the experimental range move back and forth frequently, hence they are not able to move on the substrate efficiently to make new cell-cell connections and exchange protein with new cells. On the other hand, if cells reverse with periods that are larger than the values of the experimental range, they get stuck in traffic jams, which reduces their ability to swarm efficiently, make new cell-cell connections, and spread the protein within the population. Our simulation results show that for the population of cells that reverse with periods in the experimentally observed range, the time required to reach half the maximum entropy is 84% less than that for the populations that reverse every minute, and 49% less than that for the population of cells that do not reverse at all.

Figure 2(d) shows that simulations with higher cell flexibility have a faster entropy increase in comparison with simulations with more rigid cells. The time it takes the population with experimentally calibrated cell flexibility to reach half the maximum entropy was shown to be 33% less than that for rigid cells ($k_\theta = 1$ fJ). Changing adhesion strength between cells in the range from $\epsilon = 0.001$ fJ (negligible adhesion force between two neighboring cells) to $\epsilon = 0.1$ fJ (resulting in cells sticking together after they get connected) did not have a significant impact on the efficiency of protein transfer [Fig. 2(f)], although it was shown to significantly impact the rate of cell-cell connections. As the strength of cell-cell adhesion increases, the duration of cell-cell connections increases monotonically and, as a result, stable clusters of cells are formed [Fig. 3(f)]. This suggests the existence of a balance between the rate of making cell-cell connections and the duration of the connection between two contacting cells. Relatively short cell-cell connection due to weak cell-cell adhesion leads to a higher rate of cell-cell connections with new cells, but protein cannot be exchanged efficiently because of the short connection time.

The efficiency of the protein spreading was also studied for different values of the filling fraction. Figure 2(h) shows that a monotonic increase in the filling fraction results in the monotonic increases of the efficiency of the protein spreading. This results from the formation of bacterial clusters [Fig. 3(h)] leading to an increased rate of cell-cell connections [Fig. 2(g)]. The time it takes the population with filling fraction 2% to reach half the maximum entropy is about five times longer than that for the population with filling fraction 20%.

V. CONCLUSIONS

Previous studies have demonstrated the important role of cell reversals and cell physical properties in optimizing the swarming expansion rate of an *M. xanthus* population. In this paper, we studied their impact on the rate of cell-cell connections and the spread of proteins in the population by using a detailed biologically calibrated computational model and Shannon entropy.

It has been shown experimentally that the exchange of outer membrane proteins can be beneficial to the bacterial population in several ways, such as rescuing the gliding motility of motility mutants under nutrient-rich conditions [16–18,24,25], predation [26–28], and genetic repair of damaged cells [29]. It is not currently possible to control flexibility or adhesion strength *in vivo* with an isogenic *M. xanthus* mutant strain. Therefore, a detailed computational model was used to study how quickly outer membrane (OM) protein could spread throughout the populations of *M. xanthus* A+S- mutants with different physical and behavioral properties of individual cells at the swarm edge. Cells at the swarm edge are monolayered, exposed to a maximum level of nutrient and oxygen, and behave distinctively compared to the interior cells [13,46,47]. The optimal rate of cell-cell connections and efficiency of protein transfer was obtained for reversal periods in the range from 4 to 12 min observed in experiments. This range has also been reported to optimize the expansion rate of the swarming *M. xanthus* population [13]. This suggests that swarm expansion and the efficiency of protein spreading could be related to each other. For example, optimized protein exchange and connection rate may result in more efficient motility recovery that enhances the expansion rate of the swarm, or they could be linked to an increase in the orientation correlation between bacteria [13]. However, this remains a very important open question to be investigated in future studies.

Higher cell-cell connection rates were also obtained for populations with more flexible cells. Tracking cells from *in vivo* experimental movies confirmed cells to be very flexible. Although it was shown that decreasing the strength of cell-cell adhesion increased the rate of cell-cell connections considerably, it had a negligible effect on protein spreading. Figure 3 shows that this happens because cells in a population with a high strength of cell-cell adhesion ($\epsilon = 0.1$ fJ) on average make connections that last 6.4 min, while cells in a

population with a low strength of cell-cell adhesion ($\epsilon = 0.001$ fJ) on average stay connected for about 2 min. Therefore, although a longer connection enables two connected cells efficiently to exchange their proteins, the efficiency of protein spreading at the population level is penalized by a reduction of the average rate of cell-cell connections. Consequently, the positive effect of a longer connection between cells is reduced by the decrease of the average rate of the cell-cell connections. As a result, the efficiency of the protein spreading does not depend significantly on the strength of the cell-cell adhesion.

The rate of collisions between rod-shaped particles such as *M. xanthus* can be estimated as follows by using an analogy with molecular gases: $r_c = fV\sigma/v_0$, where f is the volume fraction, V is the average particle speed, σ is the collision cross section, and v_0 is the particle volume. In two dimensions, $\sigma \approx L$, where L is the particle length, and $v_0 \approx dL$, where d is the particle width. For typical simulation conditions of $L = 5\ \mu$m, $d = 0.5\ \mu$m, $f = 0.128$, and $V = 4.3\ \mu$m/min, we obtain the collision rate $r_c \approx 1.1\ \text{min}^{-1}$. This value has the same order of magnitude as the experimentally measured connection rate R_c (see Fig. 1). It implies that under the assumption that *M. xanthus* bacteria do not follow slime trails left by other bacteria, the mechanism based on mostly uncorrelated collisions between bacteria is primarily responsible for forming connections and protein spreading.

Figure 1 shows a large increase in the value of R_c from $t_r =$ 3 to 4 min, which can be explained as follows. Cells need some minimal time to move in one direction before they reverse in order to make enough physical connections with different cells in the population to spread protein. The sum of the estimated time that two cells stay in contact (2.2 ± 0.07 min) with the time that is required for a cell to move freely before reaching another cell (1.1 ± 0.05 min) is approximately 3.3 min, which is very close to the time of the sharp increase in the value of R_c in Fig. 1.

Most bacteria grow in a mixed (and potentially hostile) environment. Many bacteria use extracellular signals via a variety of quorum sensing mechanisms to coordinate actions at the species level. However, the chemical signals for most of these quorum sensing systems are insufficient to coordinate action on time scales that lead to collective motion and swarming on surfaces. Thus the ability to use protein cues to coordinate collective actions is very appealing. In this paper, we have demonstrated that experimentally observed physical properties and multicellular behavior of *M. xanthus* favor population with an efficient spread of protein. Our findings suggest that organisms with accelerated protein spreading should have a competitive advantage in a swarm environment. Periodic reversals of movement have been reported for several bacterial species besides *M. xanthus* [48–51]. Therefore, given the importance of reversals for *M. xanthus* swarming and the potential mechanism of extracellular signaling that is investigated here, we suggest that more species might utilize periodic reversal strategies to optimize their collective behavior. Furthermore, our findings suggest that predesigned motion reversal can be employed to enhance the collective behavior of biological synthetic active systems.

ACKNOWLEDGMENTS

The research of A.A., C.W.H., A.B., J.S., and M.A. was supported by NIH Grants No. R01GM100470 and No. R01GM095959. The research of I.A. was supported by the U.S. Department of Energy (DOE): Office of Science, Basic Energy Sciences (BES), Materials Science and Engineering Division (experiment).

APPENDIX A: SHANNON ENTROPY CALCULATION

Initially N cells are randomly distributed in a two-dimensional (2D) simulation domain of the size $L_x \times L_y$. The kth cell ($1 \leqslant k \leqslant N$) is initially assigned a level of protein $n_k(t = 0) \in [0, 1]$ using a uniformly random distribution. The initial configuration of cells in the domain is shown in Fig. 4. For a system of N cells, the total amount of protein in the population is $\sum_{k=1}^{N} n_k = N/2$. The protein distribution is normalized by the total amount of protein in the population and is given by

$$\tilde{n}(k,t) = \frac{n_k(t)}{\sum_{k=1}^{N} n_k} = \frac{2n_k(t)}{N}. \tag{A1}$$

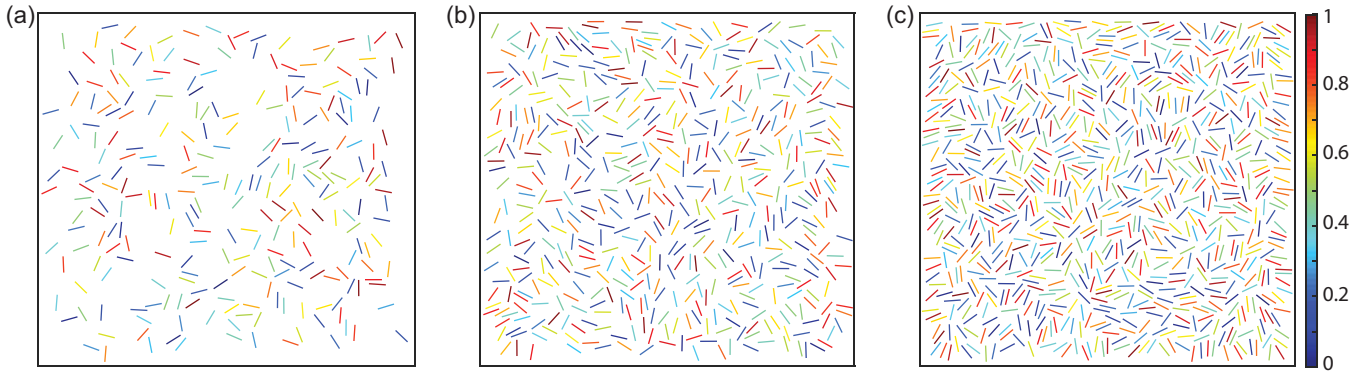

FIG. 4. Initial cell distributions in simulations of the populations with densities 6.4% (a), 12.8% (b), and 20% (c). The size of the simulation domain is set to $100 \times 100\ \mu\text{m}^2$ and the length of the cells is $5\ \mu$m. The color scale shows the level of the protein on each cell that is chosen randomly from a uniform distribution from [0, 1].

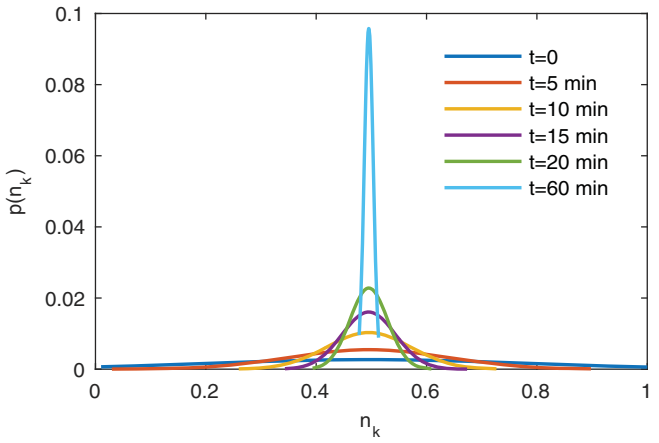

FIG. 5. Normalized protein distribution at time t. Initial protein levels of cells are chosen from a uniform random distribution. Over time, cells make connections and exchange protein with each other. The level of protein on all cells approaches the same value $n_k = 0.5$ assuming that enough time is given. Population consists of 512 cells moving inside a 2D simulation domain of the size $100 \times 100\ \mu\text{m}^2$.

The entropy of the normalized protein distribution $\tilde{n}(k,t)$ in a population at time t is defined as follows:

$$I(t) = -\sum_{k=1}^{N} \tilde{n}(k,t) \log\left(\tilde{n}(k,t)\right). \tag{A2}$$

The time evolution of the normalized protein distribution is shown in Fig. 5 for a population of 512 cells. The initial value of entropy in a population of N cells is as follows:

$$I(t=0) = -\sum_{k=1}^{N} \frac{2n_k(t=0)}{N} \log\left(\frac{2n_k(t=0)}{N}\right). \tag{A3}$$

Cells in model simulations establish physical connections with each other and exchange protein at rates observed in experiments [32]. As a result of protein exchange, the entropy of the system increases with time because mixing of protein in the population increases the uncertainty of knowing which cell has a specific level of the protein. Entropy provides a measure of uncertainty in a system. Every cell in the population will end up with the same level of protein $n_k = 0.5$ over a long enough period (Fig. 5). Therefore, given enough time, the normalized protein distribution of the population approaches the value $\tilde{n}(k) = 1/N$. As a result, the entropy of the system will reach its maximum value

$$I(t=\infty) = -\sum_{k=1}^{N} \frac{1}{N} \log\left(\frac{1}{N}\right) = \log(N). \tag{A4}$$

Therefore, in a system with N cells, the normalized entropy change from the start of the simulation (at $t = 0$) to time t is equal to $\widetilde{\Delta I}(t) = [I(t) - I(0)]/E$. The normalization factor $E = I(\infty) - I(0)$ is the maximum amount by which the entropy of the system could be increased.

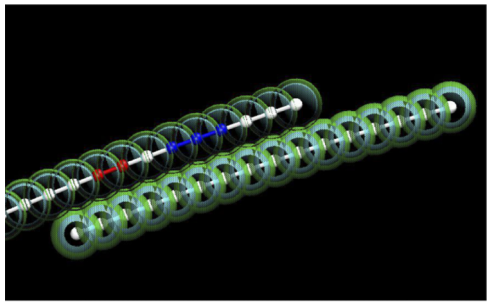

FIG. 6. Representation of cells with SCEs. White spheres and segments indicate positions and bonds of SCEs. The green (outer) shell represents the boundary for the zone of attraction, and the cyan (inner) shell represents the boundary of the repulsive force. (Repulsion and attraction zones are not to exact scale.) Red SCEs highlight stretching interactions between SCEs. Blue SCEs represent the bending interaction between SCEs.

APPENDIX B: SUBCELLULAR ELEMENT MODEL IMPLEMENTATION

1. Cell representation and subcellular element forces

The basic subcellular element (SCE) cell representation is a modification of the one used in the model described in detail in [39]. Each cell is composed of 16 SCEs that are bonded together into a string (see Fig. 6). The string consists of 15 segments, and each cell is also characterized by 14 angles between all sets of three SCEs. Segments and angles have equilibrium values $x_{\text{eq}} = \frac{\text{cell length}}{\text{number of segments}}$ and $\theta_{\text{eq}} = \pi$ and are modeled as harmonic springs with assigned stretching (k_{bond}) and bending (k_θ) coefficients. Compressibility and flexibility of a cell are determined by the values of these coefficients. The following formulas are used to describe intracellular SCE interactions:

$$E_{\text{bond}} = \tfrac{1}{2}k_b(x_{ij} - x_{\text{eq}})^2,$$
$$E_\theta = \tfrac{1}{2}k_\theta(\theta - \theta_{\text{eq}})^2.$$

Parameters were calibrated using experimental data from [39]. The interactions between neighboring cells are governed by the volume exclusion principle and adhesive interactions between individual intercellular SCEs. Interactions between the SCEs from two neighboring cells are represented by the Lennard-Jones-type potential. They are repulsive when SCEs overlap, attractive when SCEs are close but nonoverlapping, and zero when SCEs are sufficiently far apart. The strength of the interaction between the ith and jth SCEs separated by the distance x_{ij} is defined by the parameter ϵ, which is the strength of the adhesion interaction between slime capsules of the cells. The transition from repulsion to attraction takes place at the distance λ_{ij}. The value of λ_{ij} is chosen based on the known width of bacteria cells and is set to 0.5 μm. There is a cutoff distance ($\text{LJ}_{\text{cutoff}}$) that determines the maximum distance at which two SCEs interact via the nonbonded interaction potential. The SCE nonbonded interaction is described by the equation

$$E_{\text{LJ}}(\text{SCE}_i,\text{SCE}_j) = \epsilon\left[\left(\frac{\lambda_{ij}}{||x_{ij}||}\right)^{12} - \left(\frac{\lambda_{ij}}{||x_{ij}||}\right)^{6}\right]. \tag{B1}$$

The default values of the parameters used in the model are given in Table I.

2. Equations of motion

In what follows, the second term in Eq. (1) describing the potential in the paper is explained in detail. Let $\mathbf{r}_i$ be the vector pointing from SCE_i to SCE_j. Then the force $\mathbf{F}(\mathbf{x}_i)$ acting on SCE i at position $\mathbf{x}_i$ is described by

$$-\nabla_x U(\mathbf{x}_i(t)) = \mathbf{F}(\mathbf{x}(t)) = \mathbf{F}_{\mathrm{bond}} + \mathbf{F}_{\mathrm{bend}} + \mathbf{F}_{\mathrm{LJ}} + \mathbf{F}_{\mathrm{slime}},$$

where

$$\mathbf{F}_{\mathrm{bond}} = \sum_{j \in \text{bonded neighbor}} k_b(||\mathbf{x}_i - \mathbf{x}_j|| - x_{\mathrm{eq}})\hat{\mathbf{r}}_i \tag{B2}$$

and

$$\mathbf{F}_{\mathrm{LJ}} = \sum_{j \in \text{n.b. SCE}} \epsilon\left(12\frac{\lambda_{ij}^{12}}{||\mathbf{x}_i - \mathbf{x}_j||^{13}} - 6\frac{\lambda_{ij}^{6}}{||\mathbf{x}_i - \mathbf{x}_j||^{7}}\right)\hat{\mathbf{r}}_i. \tag{B3}$$

The sum in Eq. (B2) is over all bonded neighboring SCEs. All SCEs have two bonded neighbors except for the SCEs at the ends of the string representing a cell, which only have one. The list of "nonbonded SCEs" in the sum of Eq. (B3) includes all SCEs within the $\mathrm{LJ}_{\mathrm{cutoff}}$ distance of SCE i.

In a previous version of the model [39], slime propulsion was represented by the force applied to the tail SCE of a cell. In the current model, the slime propulsion is distributed in such a way that four equally spaced SCEs experience a force equal to $1/4F_s$, where $\mathbf{F}_{\mathrm{slime}} = F_s\hat{\mathbf{r}}_i$ (the direction pointing from the tail SCE to the second to last SCE). This allowed for greater flexibility of cells because in highly flexible cells, a single lagging force applied to one of the poles can cause a flailing motion. The distributed engine model is also amenable to different models of A-motility, including focal adhesion.

The angles between neighboring segments are calculated as follows. For SCEs i,j,k, where i is the SCE between j and k, $\mathbf{r}_1 = \mathbf{x}_j - \mathbf{x}_i = (dx_1, dy_1, dz_1)$ is the vector pointing from i to j and $\mathbf{r}_2 = \mathbf{x}_k - \mathbf{x}_i = (dx_2, dy_2, dz_2)$ is the vector pointing from i to k. Three components of the bending force $\mathbf{F}_{\mathrm{bend}}$ acting on the SCEs i,j,k are as follows:

$$\begin{aligned} F^n_{i\,\mathrm{bend}} &= a_n + b_n, \\ F^n_{j\,\mathrm{bend}} &= -a_n, \\ F^n_{k\,\mathrm{bend}} &= -b_n, \end{aligned}$$

where

$$\begin{aligned} a_n &= \frac{k_b\Delta\theta}{r_1 \sin\theta}\left(\frac{\mathbf{r}_2^n}{||\mathbf{r}_2||} - \cos\theta\frac{\mathbf{r}_1^n}{||\mathbf{r}_1||}\right), \\ b_n &= \frac{k_b\Delta\theta}{r_2 \sin\theta}\left(\frac{\mathbf{r}_1^n}{||\mathbf{r}_1||} - \cos\theta\frac{\mathbf{r}_2^n}{||\mathbf{r}_2||}\right). \end{aligned}$$

Three components refer to the x,y,z components of the vectors, so that $\mathbf{r}_1^1 = dx_1$, $\mathbf{r}_2^3 = dz_2$, etc. These expressions are obtained by taking the derivative of $\theta(\mathbf{r}_1,\mathbf{r}_2)$ with respect to $\mathbf{x}_i$. The forces acting on all SCEs are then determined, and Eq. (1) is integrated using the forward-Euler method

$$x(t+1) = x(t) + \frac{dt}{\gamma}[\mathbf{R}(t) - \mathbf{F}(\mathbf{x}(t))]. \tag{B4}$$

3. Protein exchange submodel

As cells i and j with protein levels $n(i)$ and $n(j)$ come into physical contact, they start exchanging protein with each other with an exchange rate R_p, as described by the following equations:

$$\begin{aligned} n(i) &= n(i) + [\bar{n} - n(i)]R_p dt, \\ n(j) &= n(j) + [\bar{n} - n(j)]R_p dt, \end{aligned} \tag{B5}$$

where $\bar{n} = [n(i) + n(j)]/2$ is the average of protein levels of cells i and j, and dt is the size of the simulation time step. The protein level on the cells is updated as long as they stay connected.

[1] T. Vicsek and A. Zafeiris, Phys. Rep. **517**, 71 (2012).
[2] D. Wall, Mol. Microbiol. **91**, 209 (2014).
[3] C. E. Shannon, Bell Syst. Tech. J. **27**, 379 (1949).
[4] A. Rhee, R. Cheong, and A. Levchenko, Phys. Biol. **9**, 045011 (2012).
[5] R. P. Mann, PLoS ONE **6**, e22827 (2011).
[6] A. Cavagna and I. Giardina, Annu. Rev. Condens. Matter Phys. **5**, 183 (2014).
[7] C. Ricotta and L. Szeidl, Theor. Popul. Biol. **70**, 237 (2006).
[8] J. He and M. W. Deem, Phys. Rev. Lett. **105**, 128102 (2010).
[9] E. Bertin, J. Phys. A **50**, 083001 (2017).
[10] M. Dworkin and D. Kaiser, *Myxobacteria* (American Society for Microbiology Press, Washington, DC, 1993).
[11] Z. Yang and P. I. Higgs, *Myxobacteria: Genomics, Cellular and Molecular Biology* (Caister Academic, Poole, UK, 2014).
[12] B. D. Blackhart and D. R. Zusman, Proc. Natl. Acad. Sci. (USA) **82**, 8767 (1985).
[13] Y. Wu, D. Kaiser, J. Yi, and M. Alber, Proc. Natl. Acad. Sci. (USA) **106**, 1222 (2009).
[14] J. Hodgkin and D. Kaiser, MGG Mol. Gen. Genet. **171**, 167 (1979).
[15] J. P. Rodriguez-soto and D. Kaiser, J. Bacteriol. **179**, 4361 (1979).
[16] A. M. Rodriguez and A. M. Spormann, J. Bacteriol. **181**, 4381 (1999).
[17] E. Nudleman, D. Wall, and D. Kaiser, Science **309**, 125 (2005).
[18] B. Jakóbczak, D. Keilberg, K. Wuichet, and L. Søgaard-Andersen, PLoS Genet. **11**, e1005341 (2015).
[19] M. Dworkin, Microbiol. Rev. **60**, 70 (1996).
[20] L. J. Shimkets, Microbiol. Rev. **54**, 473 (1990).
[21] B. Sager and D. Kaiser, Genes Dev. **8**, 2793 (1994).
[22] E. Licking, L. Gorski, and D. Kaiser, J. Bacteriol. **182**, 3553 (2000).
[23] C. W. Harvey *et al.*, PLoS Comp. Biol. **8**, e1002850 (2012).
[24] D. Pathak *et al.*, PLoS Genet. **8**, e1002626 (2012).
[25] J. Hodgkin and D. Kaiser, Proc. Natl. Acad. Sci. (USA) **74**, 2938 (1977).
[26] A. G. L. Evans *et al.*, Microbiology **158**, 2742 (2012).

[27] J. E. Berleman *et al.*, Front. Microbiol. **5**, 474 (2014).
[28] H. Zhang *et al.*, PLoS Comp. Biol. **8**, e1002715 (2012).
[29] C. Vassalo *et al.*, Proc. Natl. Acad. Sci. (USA) **112**, E2939 (2015).
[30] P. Cao, A. Dey, C. N. Vassalo, and D. Wall, J. Mol. Biol. **427**, 3709 (2015).
[31] X. Wei, D. T. Pathak, and D. Wall, Mol. Microbiol. **81**, 315 (2011).
[32] A. Ducret, B. Fleuchot, P. Bergam, and T. Mignot, eLife **2**, 2939 (2013).
[33] C. Wolgemuth, Biophys. J. **95**, 1564 (2008).
[34] A. E. Pelling, Y. Li, W. Shi, and J. K. Gimzewski, Proc. Natl. Acad. Sci. (USA) **102**, 6484 (2005).
[35] R. Balagam and O. A. Igoshin, PLoS Comp. Biol. **11**, e1004474 (2015).
[36] H. Wensink *et al.*, Proc. Natl. Acad. Sci. (USA) **109**, 14308 (2012).
[37] F. Peruani, L. Schimansky-Geier, and M. Baer, Eur. Phys. J. Spec. Top. **191**, 173 (2011).
[38] F. Peruani, J. Starruß, V. Jakovljevic, L. Søgaard-Andersen, A. Deutsch, and M. Bar, Phys. Rev. Lett. **108**, 098102 (2012).
[39] C. W. Harvey, F. Morcos, C. R. Sweet, D. Kaiser, S. Chatterjee, X. Liu, D. Z. Chen, and M. Alber, Phys. Biol. **8**, 026016 (2011).
[40] T. J. Newman, Math. Biosci. Eng. **2**, 613 (2005).
[41] S. Christley, B. Lee, X. Dai, and Q. Nie, BMC Syst. Biol. **4**, 107 (2010).
[42] C. Sweet *et al.*, J. R. Soc. Interface **8**, 1760 (2011).
[43] Z. Wu, Z. Xu, O. Kim, and M. Alber, Phil. Trans. R. Soc. A **372**, 20130380 (2014).
[44] R. Balagam *et al.*, PLoS Comp. Biol. **10**, e1003619 (2014).
[45] S. Weitz, A. Deutsch, and F. Peruani, Phys. Rev. E **92**, 012322 (2015).
[46] N. C. Darnton, L. Turner, L. Rojevsky, and H. C. Berg, Biophys. J. **98**, 2082 (2010).
[47] M. Anyan *et al.*, Proc. Natl. Acad. Sci. (USA) **111**, 18013 (2014).
[48] A. Béer, S. K. Strain, R. A. Hernández, E. Ben-Jacob, and E. L. Florin, J. Bacteriol. **195**, 2709 (2013).
[49] J. C. Lindbeck, E. A. Goulbourne, M. S. Johnson, and B. L. Taylor, Microbiology **141**, 2945 (1995).
[50] T. Kondo *et al.*, Proc. Natl. Acad. Sci. (USA) **99**, 14008 (2002).
[51] E. S. Gloag *et al.*, Proc. Natl. Acad. Sci. (USA) **110**, 11541 (2013).